A semianalytic model for photo-induced isotopic fractionation in simple molecules

Mao-Chang Liang, Geoffrey A. Blake, and Yuk L. Yung
Division of Geological and Planetary Sciences, California Institute of Technology, Pasadena, California, USA

Received 14 January 2004; revised 29 March 2004; accepted 2 April 2004; published 26 May 2004.

[1] We have developed a semianalytic model for computing the photo-induced isotopic fractionation in simple molecules of interest to the atmospheric science community. The method is based on the Born-Oppenheimer approximation and the Reflection Principle. It has the main advantage of using commonly available input data, namely, the photolysis cross sections for the standard isotopologue/isotopomer and the ground state isotope-specific spectroscopic constants. The isotopic fractionation arises principally from the spectral shift induced by the small difference in zero point energy between isotopologues/isotopomers and the contraction of the wave function due to heavier isotope substitution. The latter effect dominates photolytic fractionation away from the cross section maxima. Our new approach is demonstrated with applications to the diatomic molecules HCl and HI, and the triatomic molecules N_2O and O_3. Agreement between the model and measurements is excellent. New modeling results for the fractionation of $^{15}N^{15}N^{16}O$ in the stratosphere using the Caltech/JPL two-dimensional model are presented. *INDEX TERMS:* 0317 Atmospheric Composition and Structure: Chemical kinetic and photochemical properties; 0341 Atmospheric Composition and Structure: Middle atmosphere—constituent transport and chemistry (3334); 3210 Mathematical Geophysics: Modeling; *KEYWORDS:* atmospheres, photochemistry, stratosphere

Citation: Liang, M.-C., G. A. Blake, and Y. L. Yung (2004), A semianalytic model for photo-induced isotopic fractionation in simple molecules, *J. Geophys. Res.*, *109*, D10308, doi:10.1029/2004JD004539.

1. Introduction

[2] Stable isotopic fractionation has been known since the 1930's. Mass-dependent fractionation was first recognized by *Urey* [1947], who demonstrated that the physical basis of isotopic fractionation was "well correlated with the energy states of molecules as secured from spectral data by the use of statistical mechanics" [*Urey*, 1947, p. 563]. Subsequent work has improved the calculation of partition functions and fractionation factors [*Richet et al.*, 1977; *Kaye*, 1987].

[3] The isotopic fractionation of a trace species is diagnostic of its chemical and transport history. Stable isotopes have therefore played an important role in the quantitative understanding of atmospheric transport and chemistry. Recently, measurements of isotopic fractionation of many trace species in the terrestrial atmosphere have been reported with an accuracy <1 per mil. Examples include O_3 [*Mauersberger*, 1987; *Johnston and Thiemens*, 1997; *Mauersberger et al.*, 2001], CO_2 [*Brenninkmeijer et al.*, 1995; *Lämmerzahl et al.*, 2002], CO [*Brenninkmeijer et al.*, 1995; *Huff and Thiemens*, 1998; *Röckmann et al.*, 1999], CH_4 [*Brenninkmeijer et al.*, 1995; *Irion et al.*, 1996], and N_2O [*Yoshida and Matsuo*, 1983; *Kim and Craig*, 1993; *Cliff and Thiemens*, 1997; *Rahn and Wahlen*, 1997; *Cliff et al.*, 1999; *Yoshida and Toyoda*, 2000; *Röckmann et al.*, 2001a, 2001b]. The fractionations observed in the D/H ratio in the atmospheres of planets and satellites in the solar system have provided useful constraints on the evolution of their atmospheres [*Geiss and Reeves*, 1981; *Frost et al.*, 1982; *Owen et al.*, 1986; *Kaye*, 1987; *Owen et al.*, 1988; *Owen*, 1992; *Yung and Dissly*, 1992; *Debergh*, 1993; *Vidal-Madjar et al.*, 1998; *Yung and Kass*, 1998; *Miller and Yung*, 2000]. Most of these measurements require an understanding of the fundamental kinetic and photolytic processes that take place in the atmosphere(s) for their interpretation [e.g., *McLinden et al.*, 2003; *Morgan et al.*, 2004].

[4] Isotopic fractionation has also been extensively studied using ab initio calculations [e.g., *van Harrevelt and van Hemert*, 2000; *Johnson et al.*, 2001] and analytic models [e.g., *Yung and Miller*, 1997, hereinafter referred to as YM97; *Gao and Marcus*, 2001; *Blake et al.*, 2003]. Here, we present a semianalytic computational model of the fractionation induced by the photodissociation of simple molecules. Comparison with available laboratory data is made in section 3 and the implications for atmospheric chemistry are discussed in section 4.

2. Method

[5] In this section, we present our algorithm for calculating the dissociation cross sections of isotopically substituted species. We assume that the cross section for the standard isotopic species is known and invoke the Reflection Prin-

0148-0227/04/2004JD004539

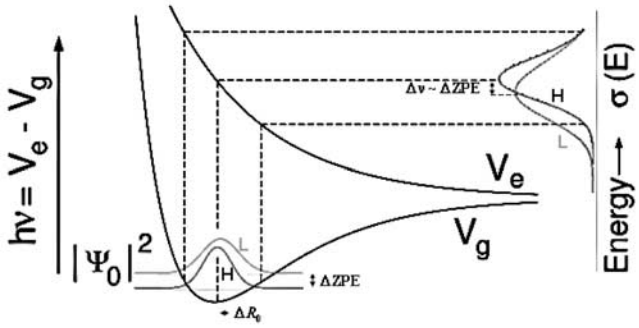

Figure 1. Schematic diagram of the direct photodissociation process, illustrating the Born-Oppenheimer approximation and the Reflection Principle (dashed lines). 'L' and 'H' refer to the standard and isotopically substituted species, respectively. Ψ_0, V_g, and V_e denote the vibrationally averaged ground state wave function, ground state electronic potential, and dissociating electronic potential, respectively.

ciple and the Born-Oppenheimer approximation to simplify the calculations. Example applications of this new method will be given in section 3.

2.1. Reflection Principle

[6] Photodissociation can be approximately classified as either direct or indirect. As a photon interacts with a molecule, absorption processes can leave it in an excited electronic state. If the lifetime of the upper state is much shorter than the vibrational period(s), the process is called direct fragmentation. If the lifetime is much longer than the vibrational period(s), the process is called indirect fragmentation. Spectroscopically, the (direct) photodissociation model presented in this work is only valid if the width of the spectrum is comfortably larger than the fundamental vibrational frequency(ies). The photodissociation cross section can thus be simply computed by mapping the square of the initial wave function onto the energy axis through the potential energy surface of the dissociative state. This is the essence of the Reflection Principle. To first order, the potential energy curve for a dissociating diatomic molecule can be represented by a linear function in the region not far from the equilibrium nuclear distance of the molecule's ground state. At sufficiently low temperatures the population of molecules in excited vibrational states is negligible, and the initial state can be approximated by the ground state wave function alone. For example, at room temperature ~90% of N_2O molecules are in the vibrational ground state and ~10% reside in the first excited bending state. Based on the Reflection Principle with a simplified upper state potential energy surface, the dissociation cross section turns out to be an energy weighted gaussian function if the initial state is the ground state - for which a simple harmonic oscillator gaussian provides a reasonable description of the true (anharmonic) wave function for small excursions from the vibrationally averaged molecular structure.

[7] A schematic of the one-dimensional Reflection Principle as applied to the direct photodissociation of diatomic molecules is illustrated in Figure 1 [cf. *Schinke*, 1993]. In the Born-Oppenheimer approximation, both the position and the momentum of the nuclei are conserved during photoexcitation. Accordingly, vertical lines can be used to map the square of the vibrational ground state wave function ($|\Psi_0|^2$) onto the energy axis (that is, the nuclear geometry remains constant). The transitions are best drawn from potential curve to potential curve (dashed lines), and the photon energy is given by $h\nu = V_e - V_g$, where V_e and V_g are the dissociative and ground state electronic potentials, respectively. Within the Born-Oppenheimer approximation, the potential curves (V_e and V_g) are independent of isotopic substitution.

2.2. Analytic Solution for Diatomic Molecules

[8] The change of mass of the isotopically substituted species from that of the more abundant standard species is usually less than 10%. This results in a small difference in the vibrational frequencies. *Yung and Miller* [1997] first modeled the fractionation in the photodissociation of nitrous oxide by shifting the whole spectrum by an amount equal to ΔZPE, where ΔZPE is the difference in zero point energy (ZPE) between the the standard species and isotopically substituted species. However, the fractionation predicted via this method is approximately half that observed in laboratory measurements and atmospheric observations. Isotopic substitution not only changes the ZPE of a given isotopologue/isotopomer, but also modifies the shape of the corresponding vibrational wave function. The modification of wave function has a significant effect on the dissociation cross section, especially away from the peak of the spectrum. Photodissociation models based on these modified wave functions have the correct form, and much more closely reproduce the laboratory measurements of isotopic fractionation [*Blake et al.*, 2003].

[9] For direct photolysis, the dissociation cross section can be approximated by the square of the transition dipole moment-weighted initial state wave function. Here we adopt the classical view of the photodissociation process to simplify the calculation: the linear momentum is independent of the spatial coordinate. The overall dissociation cross section is then the sum of all trajectories leading to the dissociation, with a particular weight for each path in phase space. The statistical weight is usually given by the Wigner distribution function [e.g., *Wigner*, 1932]. For a harmonic oscillator in the ground state, the distribution function, $P_W(R, P)$, is

$$P_W(R,P) = (\pi\hbar)^{-1} \exp\left[-2\alpha(R-R_0)^2/\hbar\right] \exp\left[-P^2/(2\alpha\hbar)\right], \quad (1)$$

where R is the instantaneous nuclear distance, P is the related linear momentum, $\hbar$ is the Planck constant, and R_0 is the vibrationally averaged nuclear distance in the ground state [e.g., *Dahl*, 1983]. For the line-width component in $P_W(R, P)$, α is defined as

$$\alpha \equiv \mu\omega/2 = \left(k/\omega^2\right)\omega/2 \propto 1/\mathrm{ZPE}, \quad (2)$$

where μ is the reduced mass, ω is the vibrational frequency, and k is the corresponding curvature of the ground potential

energy curve (the so-called spring or force constant; defined as the second derivative of V_g near R_0). The rightmost proportionality of equation (2) is given by the Born-Oppenheimer approximation, i.e., k is unchanged by isotopic substitution. This classical distribution function of the vibrational ground state is the product of two gaussians defined in phase space, one centered at the vibrationally averaged nuclear distance R_0, the other centered at $P = 0$. Since direct photodissociation occurs instantaneously in the Born-Oppenheimer approximation, the internal coordinate (R) and the corresponding momentum (P) of the parent molecule remain unchanged during the excitation process [*Mulliken*, 1971].

[10] The dissociation cross section is given by the product of the distribution function (equation (1)) and the square of the transition dipole moment. For simplicity, we first assume the transition dipole moment is independent of R, P, and isotopic substitution. The dissociation cross section σ can then be calculated as a function of photon energy E [e.g., *Schinke*, 1993] by:

$$\sigma(E) \propto E \int dP \int dR \ \exp\left[-2\alpha(R-R_0)^2/\hbar\right] \exp\left[-P^2/(2\alpha\hbar)\right] \cdot \delta(H-E), \tag{3}$$

where H is the Hamiltonian defined for the dissociative state. Note that we have omitted the square of the transition dipole moment from equation (3). By integrating equation (3), we obtain

$$\sigma(E) \propto E\alpha^{1/2} \exp\left[-2\alpha(R_t-R_0)^2/\hbar\right]/V'_{R_t} = E\beta^{1/2} \exp\left[-2\beta(E-V_0)^2/\hbar\right], \tag{4}$$

where $V_0 = V_e(R_0)$, V'_R is the absolute value of the derivative of $V_e(R)$ with respect to R, R_t is the classical turning point defined by $H(R_t, P) = E$, $\beta = \alpha/V'^2_{R_t}$, and $V'_{R_t} = V'_R|_{R_t}$. If the dissociation potential can be linearized as

$$V_e(R) \approx V_e(R_0) - V'_{R_0}(R-R_0) \equiv V_0 - V'_0(R-R_0), \tag{5}$$

the resulting σ is approximated by

$$\sigma(E) \propto E\beta^{1/2} \exp\left[-2\beta(E-V_0)^2/\hbar\right], \tag{4'}$$

where $V'_0 = V'_{R_0}$ and $\beta = \alpha/V'^2_0$. We see that the above equation is simply an energy-weighted gaussian function if the dissociating potential is linear with R. If the slope of $V_e(R)$, V'_{R_t}, is not strongly varying, that is,

$$V'_{R_t} = V'_0 + \eta, \tag{6}$$

where $\eta = \eta(R_t) \ll V'_0$, the cross section σ in equation (4) can be further simplified to

$$\sigma(E) \propto E\alpha^{1/2} \exp\left[-2\alpha(E-V_0)^2/\left(\hbar V'^2_{R_t}\right)\right]/V'_{R_t} = E\alpha^{1/2} \exp\left[-2\alpha(E-V_0)^2/\left(\hbar\left(V'_0+\eta\right)^2\right)\right]/\left(V'_0+\eta\right) \approx EG(\alpha, V_0, E)\gamma(V_0, E), \tag{7}$$

where G and γ are defined by

$$G(\alpha, V_0, E) \equiv \beta^{1/2} \exp\left[-2\beta(E-V_0)^2/\hbar\right] \tag{8}$$

$$\gamma(V_0, E) \equiv \exp\left[4\alpha_0\eta(E-V_0)^2/\left(\hbar V'^3_0\right)\right]. \tag{9}$$

The factor $\beta = \alpha/V'^2_0$ in equation (8) is used for normalization, and α_0 in equation (9) denotes the α for the standard species. Within the Born-Oppenheimer approximation and for a linearized upper state potential, isotopic substitution changes α (or β) only. The ZPE of the heavier isotopologue/isotopomer is smaller than that of the standard species. Thus, G of the heavier isotopologue/isotopomer will be narrower and sharper than that of the standard species. The function γ is equal to 1 if the dissociation potential is a linear function of the internuclear distance, i.e., $\eta = 0$, and if the dipole transition matrix element is independent of geometry. Typically, the dissociation potential is flatter and transition dipole smaller with increasing internuclear distance, and γ should therefore decrease toward larger R. If the transition dipole is assumed to vary linearly with distance and $V_e(R)$ is approximated with a quadratic function, the function γ varies as the fourth power of the transition frequency.

[11] The fractionation factor $\epsilon(E \equiv h\nu)$ is defined by the difference in cross sections between the isotopically substituted (typically with a heavier isotope, and so designated H) and standard species (or L),

$$\epsilon(E; \text{per mil}) \equiv 1000\left(\frac{\sigma_H(E)}{\sigma_L(E)} - 1\right) \approx 1000\left[\frac{G(\alpha(H), V_0(H), E)}{G(\alpha(L), V_0(L), E)} - 1\right] = 1000\left[\frac{\beta(H)^{1/2}}{\beta(L)^{1/2}} \frac{\exp\left[-2\beta(H)(E-V_0(H))^2/\hbar\right]}{\exp\left[-2\beta(L)(E-V_0(L))^2/\hbar\right]} - 1\right], \tag{10}$$

where γ is neglected since in most cases γ is much less sensitive to isotopic substitution than is G. This will be demonstrated quantitatively in section 3. Thus, the form of the isotopic fractionation induced by direct photolysis is nearly gaussian in nature, but for small effects the exponential can be expanded through the quadratic term in order to qualitatively demonstrate the effect of wave function reshaping.

[12] Both β and V_0 are isotopically sensitive, with the wavelength shift of cross section maxima related to the change in the vibrationally averaged bond length, $\Delta R_0 = R_0(L) - R_0(H)$, and the steepness of the repulsive upper state potential. For a Morse ground state potential, the change in bond length can be approximated by

$$\Delta R_0 \approx \frac{\Delta\text{ZPE}}{\text{ZPE}}\left(\frac{a_e}{4B_e}\right)R_0$$

where the rotational constant of a vibrational state i is given by $B_i = B_e + a_e\,(i + 1/2)$. The shift in energy is simply $\Delta\nu_0 \approx$

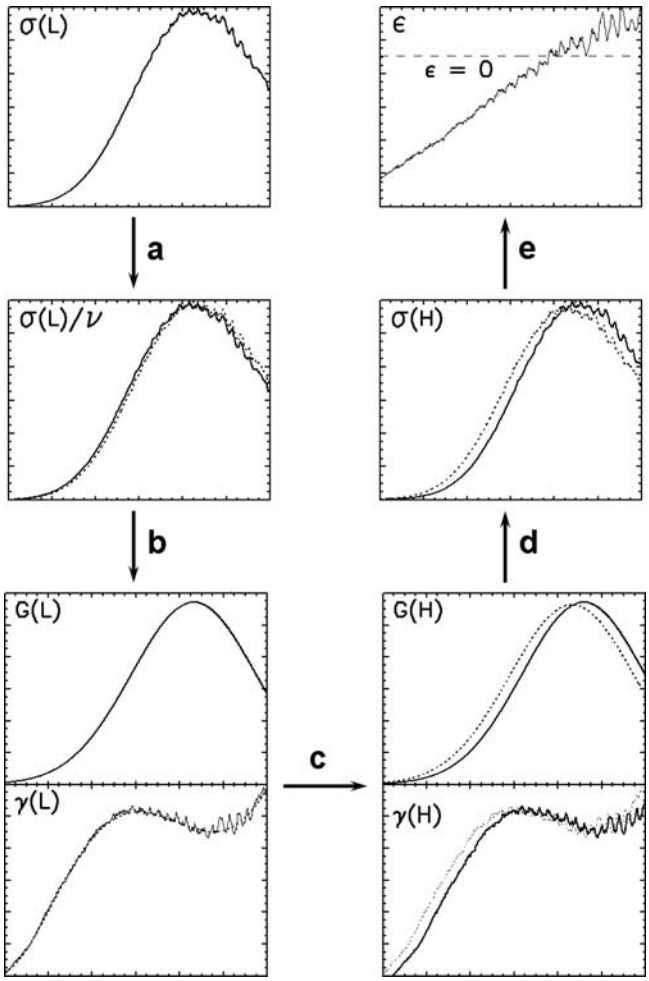

Figure 2. Schematic diagram illustrating the steps in the application of the photodissociaton model, described in section 2. The vertical axis refers to the physical quantity in the upper-left corner in each panel; the horizontal axis denotes the photon frequency ν. 'L' and 'H' denote the standard and isotopically substituted species, respectively. The full procedure is divided into five steps (a)–(e). See text for details.

$V'_0\Delta R_0$, and for HI the product $(V'_0 a_e R_0)/(4B_e\mathrm{ZPE}) = 1.03$. Thus, $\Delta\nu_0 \approx \Delta\mathrm{ZPE}$, as assumed by YM97. Using this approximation, the overall $\epsilon(\nu)$ can be written as

$$\epsilon(\nu; \text{per mil}) \approx \epsilon_1(\nu) + \epsilon_2(\nu). \tag{11}$$

Here, ϵ_1 and ϵ_2 have the approximate form

$$\epsilon_1(\nu) \equiv 1000\ \frac{1}{W^2}\Delta\mathrm{ZPE}(\nu - \nu_0 - \Delta\mathrm{ZPE}/2) \tag{11a}$$

$$\epsilon_2(\nu) \equiv 1000\frac{1}{2W^2}\frac{\Delta\mathrm{ZPE}}{\mathrm{ZPE}}(\nu - \nu_0 - \Delta\mathrm{ZPE})^2, \tag{11b}$$

where W is the full-width-half-maximum (FWHM) of the fitted gaussian function, and ν_0 is the frequency of the standard species at which the dissociation cross section is maximum. Physically, ϵ_1 follows from the shift in energy induced by the ZPE of the various species and ϵ_2 is the correction due to the change of the shape of the wave function. For large fractionation values, the full gaussian form of equation (10) should be used.

2.3. Triatomic Molecules

[13] The method developed above for diatomic molecules can be extended to triatomic compounds. There are four normal modes for linear triatomic molecules (the bending mode is doubly degenerate) and three for nonlinear triatomics. The corresponding vibrational frequencies, ω_i, for the molecules studied in this paper are tabulated in Table 1, where i equals 1, 2, and 3 for symmetric stretching, bending, and asymmetric stretching, respectively.

[14] For the photolysis of a linear molecule A-B-C $\rightarrow$ A-B + C, the following dissociation coordinate system is usually used: r, R, and θ denote the A-B bond distance, the distance between the center of mass of A-B and C, and the angle between r and R. On average, θ is zero for a linear molecule in the vibrational ground state. The dissociation potential is again expanded through its first derivatives to yield:

$$V_e(r, R, \theta) \approx V_0 - V'_r(r - r_0) - V'_R \times (R - R_0) - V'_\theta \times (\theta - \theta_0), \tag{12}$$

where the subscript "0" refers to the vibrationally averaged value, and V'_r, V'_R, and V'_θ are the partial derivatives of V_e with respect to their suffix. Within the Born-Oppenheimer approximation, the dissociation cross section can be calculated by means of the Reflection Principle and has the same form as equation (5) [cf. *Schinke*, 1993], but β must be redefined as

$$\beta = \left(V'^2_r/\alpha_r + V'^2_R/\alpha_R\right)^{-1} \tag{13}$$

for a linear molecule since the expression for the generalized β accounts only for the modes directly related to the dissociation. The bending mode, to a first approximation, is not important for linear molecules because the vibrational motion is perpendicular to the dissociation coordinate R.

Table 1. Vibrational Frequencies For HCl, HI, N_2O, and O_3[a]

Molecule		Isotopologue	ω_1	ω_2	ω_3	ZPE	ZPE′
HCl	–	^{1}HCl	2964.5	...	...	1482.3	1482.3
	–	^{2}DCl	2131.6	...	...	1065.8	1065.8
HI	–	^{1}HI	2289.2	...	...	1144.6	1144.6
	–	^{2}DI	1629.7	...	...	814.9	814.9
N_2O	–	$^{14}N^{14}N^{16}O$	1284.9	588.7	2223.8	2343.1	1754.3
	–	$^{14}N^{14}N^{17}O$	1264.7	586.3	2220.1	2328.7	1742.4
	–	$^{14}N^{14}N^{18}O$	1246.9	584.1	2216.7	2315.9	1731.8
	–	$^{15}N^{14}N^{16}O$	1280.4	575.5	2177.7	2321.1	1735.8
	–	$^{14}N^{15}N^{16}O$	1269.9	585.3	2201.6	2304.5	1729.0
	–	$^{15}N^{15}N^{16}O$	1265.3	571.9	2154.7	2281.9	1710.0
O_3	–	$^{16}O^{16}O^{16}O$	1103.1	700.9	1042.1	1423.1	1423.1
	–	$^{16}O^{16}O^{17}O$	1095.7	692.4	1035.4	1411.7	1411.7
	–	$^{16}O^{16}O^{18}O$	1090.4	684.6	1028.1	1401.5	1401.5
	–	$^{16}O^{17}O^{16}O$	1087.8	697.1	1024.4	1404.7	1404.7
	–	$^{16}O^{18}O^{16}O$	1074.3	693.3	1008.5	1388.0	1388.0
	–	$^{18}O^{18}O^{18}O$	1041.6	661.5	984.8	1343.9	1343.9

[a]The units are in cm^{-1}.

The α_r and α_R are defined in accordance with equation (2), and so may be simply related to the ZPE, or

$$\beta^{-1} = \sum V_i'^2/\alpha_i \propto \sum (V_i'^2/k_i)\omega_i \propto \sum \omega_i = \mathrm{ZPE}', \quad (14)$$

if the prefactors $(V_i'^2/k_i)$ in front of ω_i are the same, where α_i is the α for each normal mode, and ZPE′ is the sum of all vibrational frequencies significantly participating in the dissociation ($\omega_1 + \omega_3$ for a linear molecule). The fractionation factor ϵ for a linear molecule is thus analogous to equation (10). Expanded through the quadratic term, ϵ can again be represented by

$$\epsilon(\nu; \text{per mil}) \approx \epsilon_1(\nu) + \epsilon_2'(\nu), \quad (15)$$

where ϵ_1 is defined as in equation (11a) and ϵ_2' is given by

$$\epsilon_2'(\nu) \equiv 1000 \frac{1}{2W^2} \frac{\Delta\mathrm{ZPE}'}{\mathrm{ZPE}'} (\nu - \nu_0 - \Delta\mathrm{ZPE})^2.$$

ΔZPE′ is the difference of ZPE′ between the standard species and the isotopically substituted species.

[15] For a nonlinear molecule, the bending mode is no longer perpendicular to R. We amend equations (13) and (14), for which the bending mode contribution must be included in β, which is redefined by

$$\beta = \left(V_r'^2/\alpha_r + V_R'^2/\alpha_R + V_\theta^2/\alpha_\theta\right)^{-1}. \quad (16)$$

The fractionation factor ϵ is the same as that defined in equation (15), but now ZPE′ and ΔZPE′ are equal to ZPE and ΔZPE, respectively. The summation in equation (14) for nonlinear molecules thus runs over all the vibrational frequencies. Note that the above calculations are valid only for the dissociation process A-B-C → A-B + C, and cannot be used to describe the A-B-C → A-C + B channel. The latter is much less likely so we will not consider it here. For example, in the photolysis of water and nitrous oxide, the channels $H_2O \rightarrow OH + H$ and $N_2O \rightarrow N_2 + O(^1D)$ account for essentially 100% for the dissociation.

[16] As shown schematically in Figure 2, in actual practice the calculation of isotopic fractionation from the known dissociation cross section of the standard species is divided into five steps:

[17] 1. The dissociation cross section of the standard isotopologue/isotopomer is divided by the corresponding dissociating photon frequency ν (see equation (7)) to obtain σ/ν.

[18] 2. The experimental values of σ/ν from (a) are then fitted with a three-parameter gaussian function, yielding a best guess for the wave function G. Values of γ are obtained from the ratio of σ/ν to G, as described in equations (7)–(9), and then fitted to a fourth-order polynomial (shown in dotted line).

[19] 3. Once derived, the functional forms of G and γ are derived for the isotopically substituted species using the values of ZPE and ZPE′ tabulated in Table 1. As a guide to the reader, schematic illustrations of G and γ for the standard and substituted species are shown with the dotted and solid lines, respectively.

[20] 4. The photodissociation cross section for the isotopically substituted species is then constructed by multiplying G, γ, and ν. In the figure, the dotted line again shows the dissociation cross section of the standard species for comparison.

[21] 5. Finally, the fractionation factor ϵ is calculated from equation (10).

2.4. Temperature Dependence

[22] Temperature-Independent Model: Typical atmospheric chemical reactions take place at <300 K, and we can often assume that all the molecules lie in the ground state. According to equation (7), in such cases the measured cross section can be fitted by G and γ, and the resulting fractionation can be calculated from equation (15) with an appropriate adjustment of ZPE′ (tabulated in Table 1).

[23] Temperature-Dependent Model: In some molecules, the dissociation cross section of the standard species has been measured at more than one temperature, permitting the influence of vibrationally excited states to be directly examined. The contribution from each state can be approximated by the assumption of statistical equilibrium [e.g., *Selwyn and Johnston*, 1981]. At room temperature or below, levels up to the second excited state of the lowest energy vibration typically capture nearly all of the total population. The dissociation is the sum of the contributions from these three states:

$$\sigma(T, \nu) = \sum_i g_i(T)\sigma_i(\nu) \quad (17)$$

$$\sum_i g_i(T) = 1 \quad (17a)$$

where the subscript i ranges from 0 to 2 (vibrational ground state to second vibrational excited state) and $g_i(T)$ is the population weighting for the i-th state at temperature T. The fractionation factor ϵ is expressed by

$$\epsilon(T, \nu; \text{per mil}) \approx 1000\left[f\frac{g_0(H)G_0(H) + g_1(H)G_1(H) + g_2(H)G_2(H)}{g_0(L)G_0(L) + g_1(L)G_1(L) + g_2(L)G_2(L)} - 1\right], \quad (18)$$

where f is a scaling factor, which is energy independent and can be determined when the fractionation factor has been measured at any one temperature or from the temperature-independent model. Physically, this factor accounts for subtle variations in the transition dipole surface or anharmonicities in the actual bound state wave functions. Such variations are ignored in equations (10) and (18), but manifest themselves in the differing γ shown in Figures 3, 4, and 7.

3. Applications

3.1. Diatomic Molecules: HCl and HI

[24] Diatomic molecules form the simplest tests of the Born-Oppenheimer photolysis model, and here HCl/DCl and HI/DI are used for a quantitative demonstration of our approach. Strictly speaking, HCl and HI do not follow the assumptions laid out in section 2, in that there are two upper

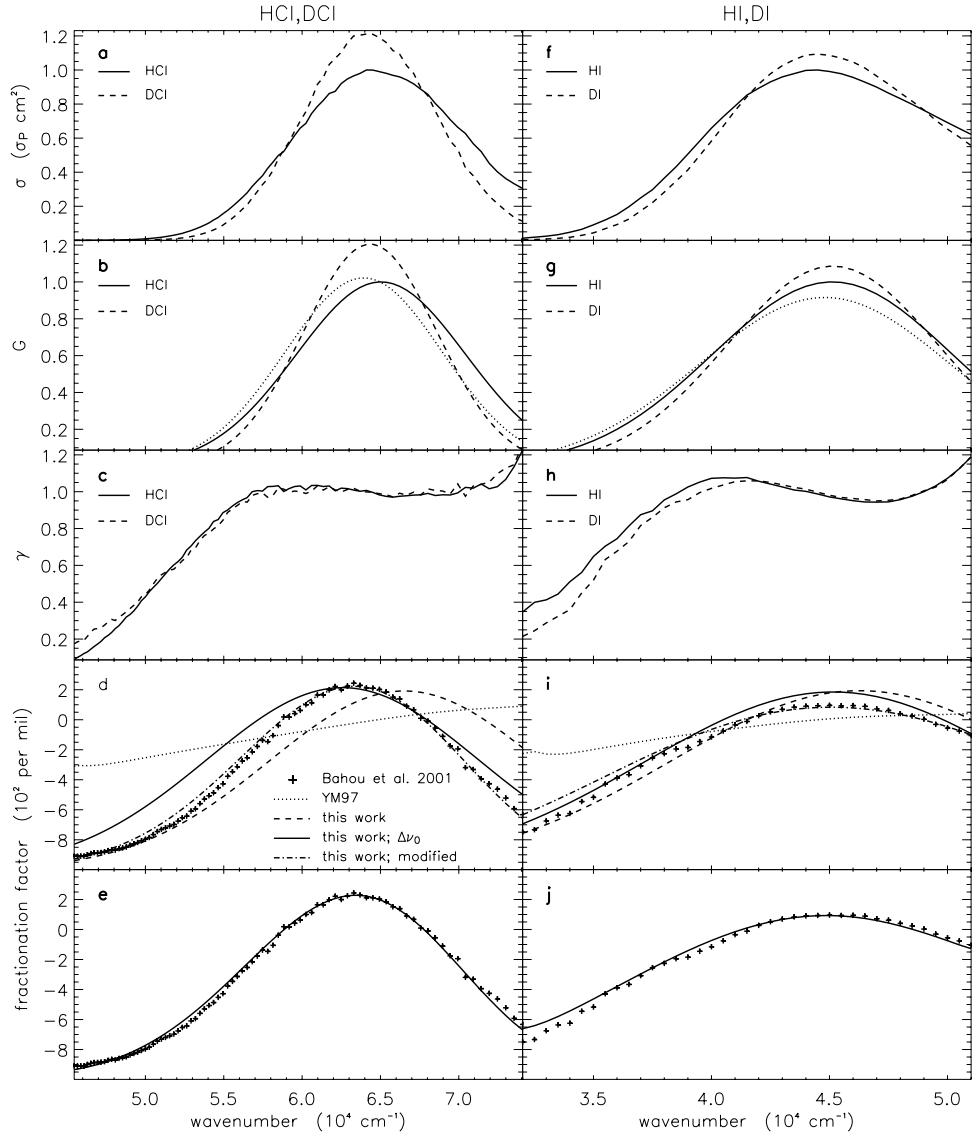

Figure 3. Applications of the new photodissociation algorithm to the diatomic molecules HCl/DCl and HI/DI. The first three panels present the decomposition of the individual cross sections into their isotope-dependent (G) and isotope-independent (γ) components. The bottom two panels present various fits to the D/H fractionation factor(s). The dissociation cross sections in Figures 3a and 3f have been divided by the maximum cross sections of the standard species HCl and HI, with $\sigma_P = 3.4 \times 10^{-18}$ cm^2 and $\sigma_P = 8.2 \times 10^{-18}$ cm^2, respectively. The various model fits in Figures 3d and 3i denote the state decomposition from the spin-orbit coupling of Cl and I. The final fits incorporating γ are given in Figures 3e and 3j.

states thanks to the strong spin-orbit interactions in Cl and I. As a result of these interactions, there are two channels ($^2P_{3/2}$ and $^2P_{1/2}$) leading to the dissociation of the parent molecule [e.g., *Ascenzi et al.*, 1999; *Brown and Balint-Kurti*, 2000]. The branching ratio for the dissociation of heavier isotopologue (DCl and DI) via the excited state $^2P_{1/2}$ channel of Cl/I is smaller as a consequence of the increased adiabaticity of the DCl/DI photodissociation (thanks to the slower relative speed between D and Cl/I as compared to H and Cl/I for the same kinetic energy). This spin-orbit coupling means that two states must be considered in the photodissociation process, with different branching ratios as a function of hydrogen isotopic substitution. We will address these complications below, but first proceed with the formalism developed in section 2.2 since it captures the essential details of the isotopic behavior of hydrogen halide photodissociation.

[25] Figure 3a shows the measured dissociation cross sections σ for HCl and DCl [*Bahou et al.*, 2001]. These cross sections have been normalized by the peak cross section of HCl, σ_P, where $\sigma_P = 3.4 \times 10^{-18}$ cm^2. The first step in computing the DCl cross section is to employ equation (7), which consists of three factors, $E \equiv h\nu$, G, and γ. In order to obtain G in equation (8), the normalized dissociation cross section is divided by the photon energy ν. The resulting data are then fitted by a gaussian with parameters ν_0, W, and the peak amplitude (see Figure 3b), whose values are tabulated in Table 2.

Table 2. Parameters Obtained From Gaussian Fitting[a]

Molecule		Isotopologue	ν_0	W	Amplitude
HCl	–	^{1}HCl	65034.6	5401.1	1.000
	–	^{2}DCl	64345.7	4252.1	1.205
HI	–	^{1}HI	45123.8	5085.7	1.000
	–	^{2}DI	45133.3	4469.0	1.085
N_2O	–	$^{14}N^{14}N^{16}O$	55027.7	3321.7	1.000
O_3	–	$^{16}O^{16}O^{16}O$	39291.1	2586.5	1.000
	–	$^{18}O^{18}O^{18}O$	39383.9	2514.6	1.052

[a]The units for ν_0 and W are in cm^{-1}. The amplitude of the isotopically substituted species has been normalized by that of the standard species.

[26] As Figures 3a and 3b show, the DCl spectrum has a higher peak and narrower width than that of HCl. This result is consistent with equation (8), in which the shape of the spectrum reflects the shape of the ground state wave function within the Born-Oppenheimer approximation. Figure 3c shows the respective $\gamma(\nu)$ which are computed as the ratio $\sigma/(EG)$. Near the peak of the dissociation cross section, $\gamma \approx 1$. As anticipated by equation (9), in which η is more (positive) negative at higher (lower) energies, $\gamma < 1$ to the far red of the cross section maxima and >1 to the blue.

[27] The same analysis is applied to HI and DI and is shown in Figures 3f, 3g, and 3h. The dissociation cross sections of HI and DI have been measured by *Ogilvie* [1971]. Here they have been normalized to the HI cross section peak, $\sigma_P = 220$ mol^{-1} cm^{-1} = 8.2 $\times$ 10^{-18} cm^2. Note that the γ for the standard species, HCl and HI, is not so different from that for the isotopically substituted species, DCl and DI, as expected. At energies far from the peak of the cross section, the change of G between isotopologues is much more significant than that of γ, and it is therefore safe to omit γ [as in equation (10)] for the computation of ϵ. Figures 3d and 3i show the fractionation factor ϵ for HCl/DCl and HI/DI. The dashed line shows the predicted ϵ using equation (10), with the YM97 ZPE model shown for comparison (dotted line). The results using our new method have the right form and magnitude to fit to the measured ϵ (cross symbol), but the predictions are shifted in energy with respect to the measurements thanks to the two spin-orbit states of the dissociating potential. The solid line depicts the prediction when adopting the experimental cross section maxima for the ΔZPE in equation (11a); the computation of the shape of the isotopically substituted spectrum still follows the scheme described in section 2.

[28] The spin-orbit splitting is not large enough to resolve spectrally, but is manifest as a blueshift of the HCl/HI dissociation spectrum relative to that of DCl/DI thanks to the increased importance of the excited halogen $^2P_{1/2}$ channel. This blueshift is quite noticeable for HCl/DCl (see Figure 3a), while the peak positions of the dissociation cross sections of HI and DI are comparable (Figure 3f).

[29] If we assume that the dissociations of DCl and DI are fully adiabatic, that is, that the DCl/DI dissociation occurs only via the ground $^2P_{3/2}$ channel of Cl/I, then the dissociation cross section of HCl/HI via the ground Cl/I channel can be calculated from the DCl/DI dissociation cross section by means of equation (7). The actual branching ratio of the dissociation of DCl via the excited Cl channel is $\sim$0.2 at $\sim$193 nm [see *Tonokura et al.*, 1992], and so this approximation should be a good first step. The expected G of HCl dissociation via the ground Cl channel is represented by equation (8) and shown by the dotted line in Figure 3b. The branching ratio of HCl via the excited Cl channel is $\sim$0.3 overall [*Tonokura et al.*, 1992], and the contribution from the excited Cl channel can be computed by the difference of HCl's G and the G via the ground state Cl channel. Gaussian fits to the spectra so obtained yield peaks offset by $\sim$3700 cm^{-1}, and the width is increased by $\sim$7% relative to that of the ground state. We note that the change of the width may be due to the change of the slope in the dissociation potential surface. The fitted values are tabulated in Table 3. As the dash-dotted line of Figure 3d shows the resulting ϵ is in excellent agreement with measurements. In fact, ϵ is simply the fractionation of the fitted G between HCl and DCl because the nongaussian γ function is largely insensitive to isotopic substitution (e.g., Figure 3c).

[30] The same algorithm is applied to HI and DI and the results are shown in Figures 3f–3i. By considering the two dissociation channels for HI/DI, the improvement of ϵ (shown in dash-dotted line) is not as great as that for HCl/DCl simply because HI/DI photodissociation is more adiabatic than that for HCl/DCl. The greater error of HI/DI at low energy end is due to the neglect of γ. The spectra of γ for HI and DI are shown in Figure 3h: the difference at low energy end is clearly somewhat greater than that for HCl and DCl. When including γ, as described in equations (7) and (9), the predicted ϵ matches the measurements well, as shown in Figures 3e and 3j. The lowest energies correspond to the largest internuclear distances where the effects of anharmonicity are greatest. Improved fits should therefore be possible with numerical wave functions derived from fits to the full suite of isotope specific rovibrational spectroscopic constants.

3.2. Linear Triatomic Molecule: N_2O

[31] The cross sections of $^{14}N^{14}N^{16}O$ have been examined by many authors. Here we use the measurements of *Selwyn and Johnston* [1981], *Yoshino et al.* [1984], and *Merienne et al.* [1990]. *Yoshino et al.* [1984] measured the cross section in the wavelength range 170–222 nm at room temperature, their results are shown in Figure 4. The cross section has been normalized to the peak of the $^{14}N^{14}N^{16}O$ spectrum, $\sigma_P = 1.4 \times 10^{-18}$ cm^2. The Yoshino et al. cross sections are first used to determine those of the other isotopologues/isotopomers by means of the temperature-independent model (section 2.4), with the room temperature results presented in Figure 5. Our prediction (solid line) is in good agreement with the measurements. YM97's ZPE model and the *Johnson et al.* [2001] ab initio model are shown for comparison. YM97's model underestimates ϵ by more than a factor of 2, while Johnson et al.'s ab initio calculations agree well with the measurements except for 546 and 556. The ab initio prediction of ϵ for 546 is even

Table 3. Parameters for HCl and HI at Two Dissociation Channels[a]

Molecule	ν_0^1	W^1	ν_0^2	W^2
HCl	63929.9	5017.1	67599.2	5369.7
HI	44803.6	5296.6	45621.5	4644

[a]The superscripts 1 and 2 are for the dissociation via the ground Cl and excited Cl channels, respectively. The decomposition is based on the adiabatic dissociation of DCl and DI with the branching ratio of 0.3 for HCl and HI via the excited Cl/I channel.

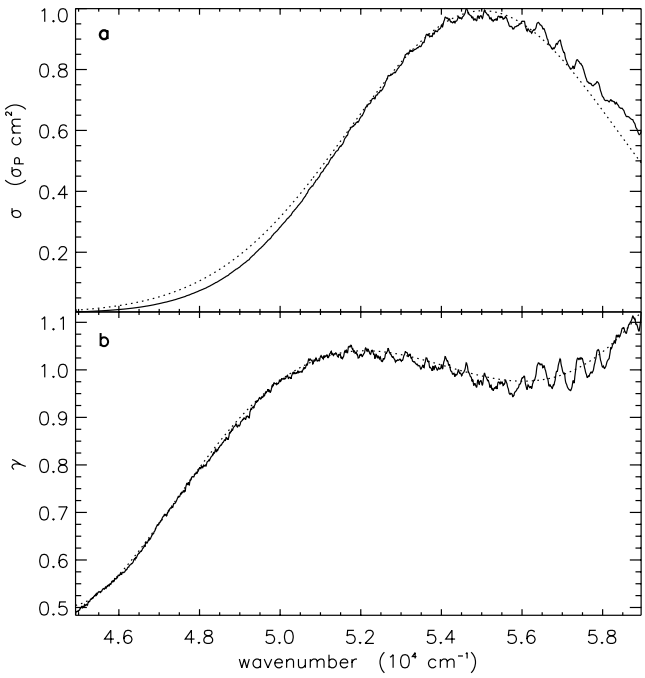

Figure 4. (a) The $^{14}N^{14}N^{16}O$ photodissociation cross section, measured by *Yoshino et al.* [1984] at 295 k, and normalized to the peak $\sigma_P = 1.4 \times 10^{-18}$ cm^2. The gaussian fit is shown by the dotted line. (b) The form of γ for N_2O. A fourth-order polynomial fit is shown by the dotted line, which has a functionally similar to the HCl and HI systems (see Figures 3c and 3h).

worse than YM97's, most likely due to the assumption of a fixed N-N bond length in the dissociation process [*McLinden et al.*, 2003]. Our prediction underestimates ϵ by 10–20 per mil for 456 and ~15% for 556. According to equation (4), the dissociation cross section is determined by the slope of the dissociation potential and the gaussian width of the ground state wave function. So, if the Born-Oppenheimer approximation is invalid (thanks to curve crossings in the excited state, for example), the prediction of ϵ will be accordingly imprecise. Nonuniform prefactors in front of the ω_i in equation (14) may also contribute to this underestimation.

[32] This simple one-state model cannot account for the cross section variations seen in the laboratory. *Selwyn and Johnston* [1981], for example, measured cross sections over the wavelength range 172–197 nm at six temperatures, ranging from 150–500 K; while *Merienne et al.* [1990] carried out measurements over the wavelength range 200–240 nm at 3 temperatures, ranging from 220–296 K. The combined data [*Selwyn and Johnston*, 1981; *Merienne et al.*, 1990] yields temperature-independent cross sections for three vibrational states [*Selwyn and Johnston*, 1981]. The application of the temperature-dependent fractionation approach to N_2O is shown in Figure 6, where $^{14}N^{14}N^{16}O$, $^{14}N^{14}N^{18}O$, $^{15}N^{14}N^{16}O$, $^{14}N^{15}N^{16}O$, and $^{15}N^{15}N^{16}O$ are renamed 446, 448, 546, 456, and 556 for simplicity.

[33] Figure 6 shows the predicted fractionation factor at 295 and 233 K using the temperature-dependent model described in section 2.4. Parameters for the state-decomposed cross sections and scaling factors f are given in Table 4. The latter account for small dipole moment surface variations with isotopic substitution. Our predictions are in good agreement with the ab initio calculations except for 546 and 556. The prediction for 556 at 233 K reproduces well the single mass spectrometric measurement from laboratory photolysis experiments [*Kaiser et al.*, 2003], and implies the algorithm and the assumption of ZPE′ and ΔZPE′ (cf. section 2.4) used to calculate the cross sections as well as the fractionation factors are reasonable.

3.3. Nonlinear Triatomic Molecule: O_3

[34] The dissociation cross sections of $^{16}O^{16}O^{16}O$ (666) and $^{18}O^{18}O^{18}O$ (888) have been measured by *Parisse et al.* [1996] at 295 K and are shown in Figure 7. Here the cross sections have been normalized to the peak value of σ(666), $\sigma_P = 1.2 \times 10^{-17}$ cm^2. Our model as well as YM97's ZPE model is applied, with results shown in Figure 8. O_3 is a nonlinear molecule, and so the reshaping of the wave function uses the full ΔZPE's since all three vibrational modes contribute significantly to the dissociation. The prediction of our model for 888 is in excellent agreement with the measurements. Figure 8 shows the fractionation factors for 667 ($^{16}O^{16}O^{17}O$), 676 ($^{16}O^{17}O^{16}O$), 668

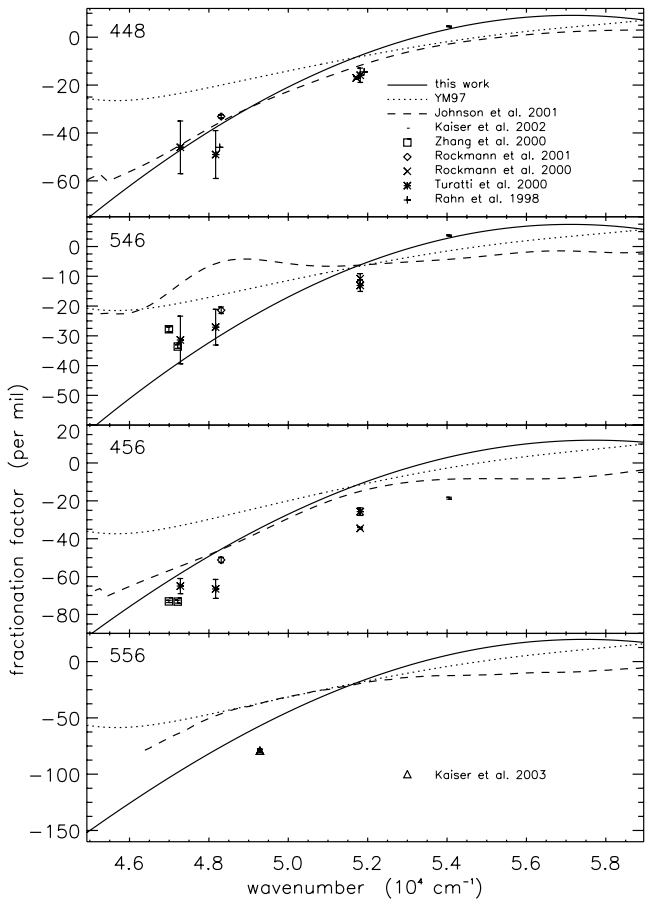

Figure 5. Comparison of the predicted ϵ using our new algorithm to YM97's ZPE model, *Johnson et al.*'s [2001] ab initio calculation, and laboratory measurements (with 2-σ error bar overplotted) for four N_2O isotopologues/isotopomers. The solid curve depicts the temperature-independent model described in section 2.4.

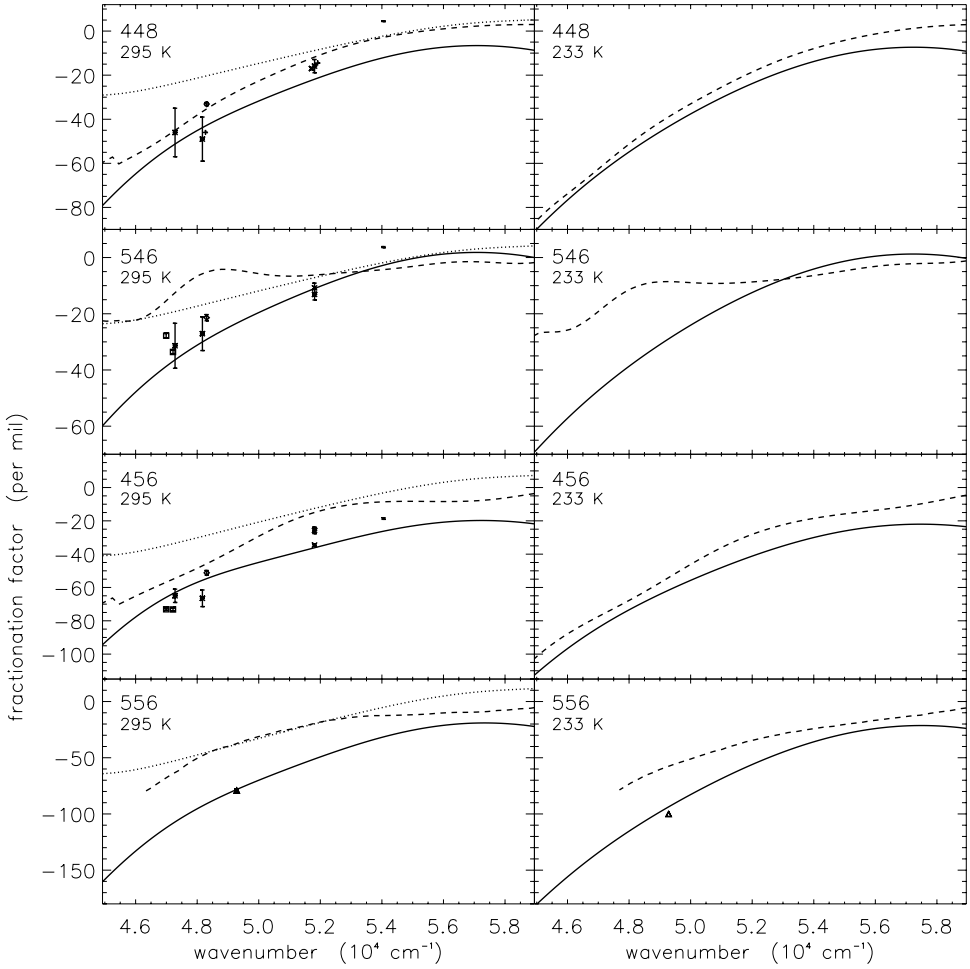

Figure 6. Comparison of the temperature dependence of ϵ using the three state temperature-dependent model (section 2.4) to *Johnson et al.*'s [2001] ab initio calculation for N_2O isotopologues/isotopomers at 295 and 233 K.

($^{16}O^{16}O^{18}O$), 686 ($^{16}O^{18}O^{16}O$), and 888. The results show that the heavier isotopologues/isotopomers are substantially enriched by long wavelength ozone photolysis, with values that are significantly underestimated by the YM97 ZPE model.

4. Applications to the Atmosphere

[35] Isotopic fractionation in the atmosphere plays an important role in constraining sources and sinks of atmospheric gases and for tracing the evolution of the atmosphere. Here we will briefly discuss some of the applications of this work.

[36] HCl: Hydrogen chloride was discovered in the Venusian atmosphere at altitudes above the clouds (>65 km above the surface) [*Connes et al.*, 1967], and the photochemistry of HCl has been studied extensively since then [*Prinn*, 1971; *McElroy et al.*, 1973; *Yung and DeMore*, 1982; *Bahou et al.*, 2001]. The observed D/H ratio in the Venusian atmosphere is nearly 100 times greater than that in the terrestrial atmosphere [e.g., *Donahue et al.*, 1982; *McElroy et al.*, 1982]. Since the water vapor in the Venusian atmosphere is trapped below 60 km, mainly by H_2SO_4, the major carrier of H in the upper atmosphere is HCl. Hence the enrichment of deuterium in the Venusian atmosphere may be due the photolytic fractionation between DCl and HCl. Indeed, the photolytic rate of DCl turns out to be only 16% that HCl for the conditions above the cloud layer [*Bahou et al.*, 2001]. This difference in the photolytic rates may contribute significantly to the enhancement of D/H ratio in the Venusian atmosphere.

[37] HI: Despite the importance of iodine chemistry in the terrestrial atmosphere [e.g., *Vogt et al.*, 1999], neither HI nor DI has been measured. We hope this work may stimulate interest in these two species.

[38] N_2O: Nitrous oxide is a potent greenhouse molecule as well as the major source of NO_x in the upper atmosphere.

Table 4. Parameters for Decomposed Cross Section and *f* Factor of N_2O[a]

State	Amplitude	ν_0	W
0	1.00	55450.5	3166.3
1	3.46	54536.7	3105.4
2	3.51	50165.0	2338.7

Species	448	546	456	556
f	0.981	0.992	0.960	0.953

[a]The peak amplitude of the vibrational ground state (0) is 1.2×10^{-19} cm^2.

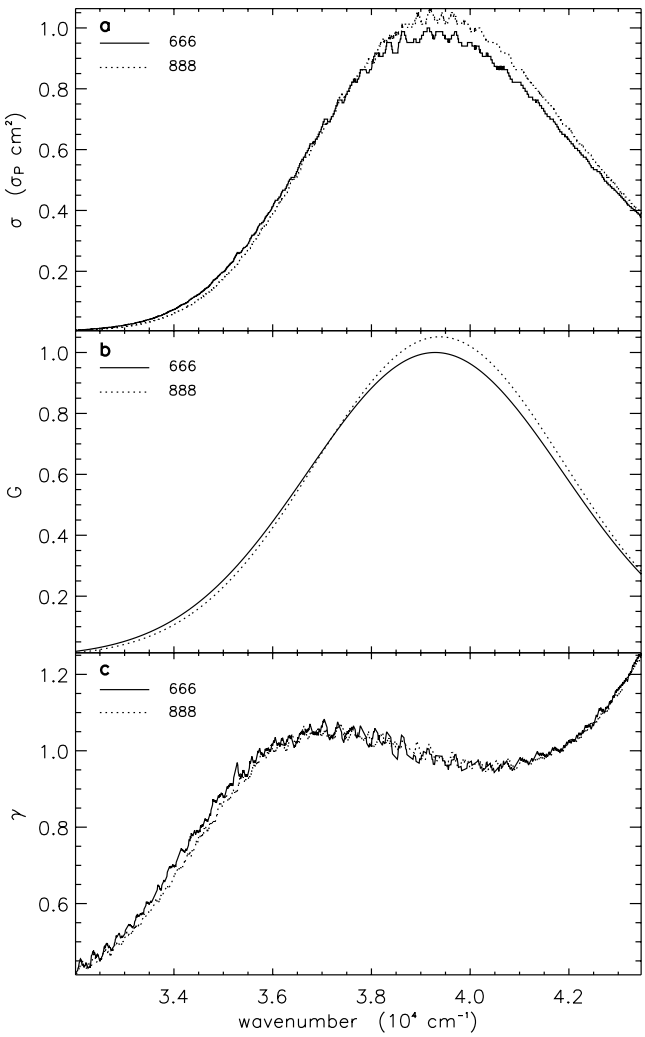

Figure 7. (a) The dissociation cross sections of $^{16}O^{16}O^{16}O$ and $^{18}O^{18}O^{18}O$, as measured by *Parisse et al.* [1996], at 295 K, and normalized to $\sigma_P = 1.2 \times 10^{-17}$ cm^2. (b) The decomposed γ.

It is produced mainly from land (~2/3) and oceanic microbial activity (~1/3) as a by-product of nitrification and denitrification reactions. Human activity plays an important role in the N_2O budget, in which about one-third of the current emissions are anthropogenic [*Intergovernmental Panel on Climate Change* (*IPCC*), 2001]. The isotopic composition of N_2O has been extensively studied [*Yoshida and Matsuo*, 1983; *Kim and Craig*, 1993; *Cliff and Thiemens*, 1997; *Rahn and Wahlen*, 1997; *Cliff et al.*, 1999; *Yoshida and Toyoda*, 2000; *Röckmann et al.*, 2001a, 2001b], and global modeling has been carried out to determine the spatial distribution, isotopic fractionation and budget of N_2O [*McLinden et al.*, 2003; *Morgan et al.*, 2004]. However, only singly substituted isotopologues/isotopomers, 456, 546, 447, 448, have been modeled to date.

[39] Here, we extend the modeling to a doubly substituted isotopologue, 556. Our newly developed model is in good agreement with the measurements (compare Figures 5 and 6). The application to the Earth's stratosphere was carried out using the Caltech/JPL two-dimensional KINETICS model with an appropriate stream function. A detailed description of this model has been given in *Morgan et al.* [2004]. As shown in Figure 9, 556 is ~50% more enriched than 456 both in the lower stratosphere and in the upper stratosphere. Lower and upper stratospheric regions were separated at $ln(f) = -0.6$, where f is the ratio of the remaining N_2O to that of the initial N_2O in the upwelling air parcel. As expected, the enrichment of this doubly substituted species is larger than those of singly substituted species, and reflects the fractionation levels induced by photolysis in both the 456 and 546 isotopologues [*Kaiser et al.*, 2003]. The latest generation of multi-collector stable isotope mass spectrometers are certainly capable of making high precision measurements on multiply substituted atmospheric trace gases [*Eiler and Schauble*, 2004], but our predicted results remain to be verified by atmospheric measurements. Further, we know little about the biological production of doubly substituted N_2O. The major production mechanisms are nitrification and denitrification, with distinctive isotopic signatures [see *Stein and Yung*, 2003]. The doubly substituted species may offer additional information of the dependence of the production of N_2O as a function of the environmental conditions such as temperature, pH, and oxidation state. New laboratory measurements are needed to establish these fractionation patterns.

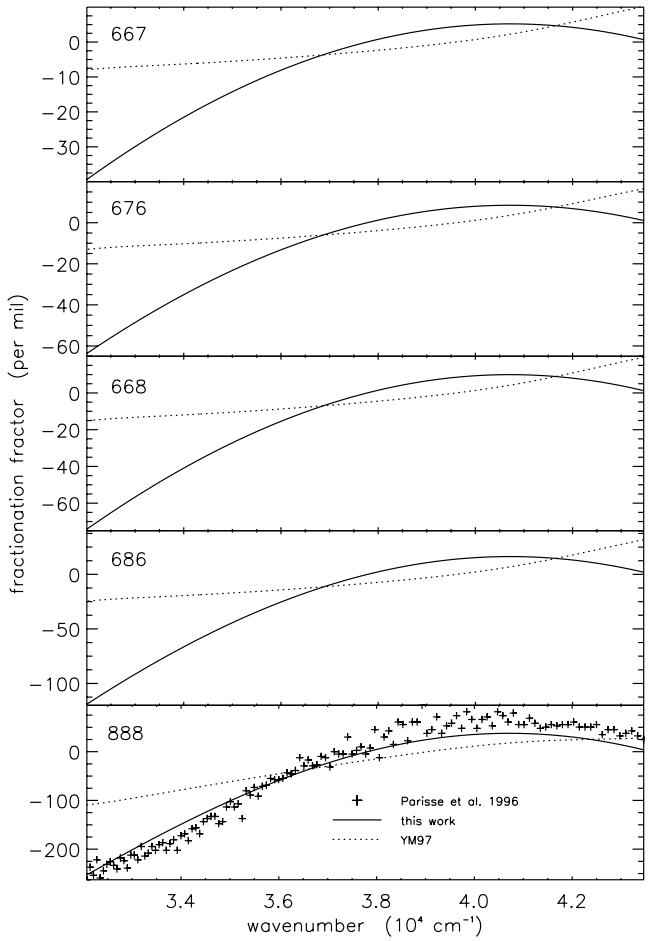

Figure 8. Comparison of the predicted ϵ to YM97's ZPE model and laboratory measurements [*Parisse et al.*, 1996] for O_3 isotopologues/isotopomers.

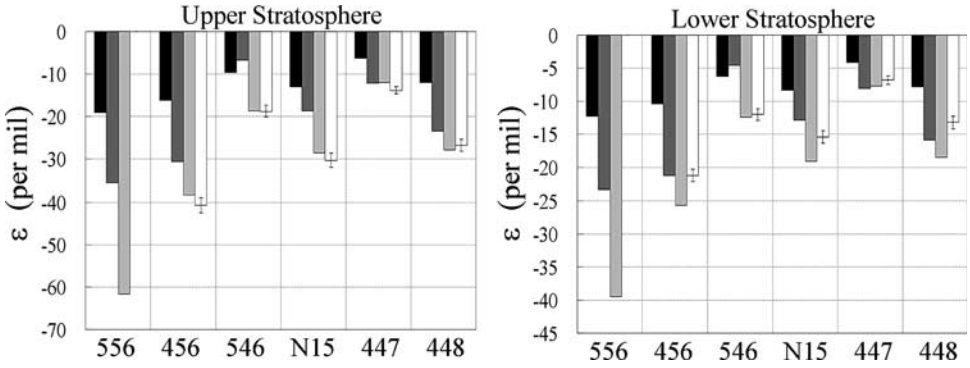

Figure 9. Applications of the predicted fractionations of the dissociation cross sections of nitrous oxide's isotopologues/isotopomers in the Earth's lower and upper stratosphere. $ln(f) = -0.6$ was used to delineate the boundary, where f is the ratio of the remaining N_2O to that of the initial N_2O in the upwelling air parcel. White bar: atmospheric measurements, with 1 σ error bars overplotted. Light gray bar: this work. Dark gray bar: *Johnson et al.*'s [2001] ab initio calculations. Black bar: The ZPE model of YM97.

[40] O_3: The roles of O_3 as UV shield and as a greenhouse gas are well known. The production rate of O_3 in the stratosphere is mass-independent (i.e., $\delta^{17}O \approx \delta^{18}O$) and a chemical mechanism consistent with these properties has been identified by *Gao and Marcus* [2001]. In the stratosphere, the photo-induced isotopic fractionation for O_3 is clearly mass-dependent, according to our model. The conclusion is robust since the prediction for 888 is in excellent agreement with the laboratory measurements (cf. Figure 8). Interestingly, the isotopomer dependence (686 versus 668, for example) of photolysis is opposite to that of the chemical reactions which form ozone. As a result, both the overall fractionation and the isotopic patterns in the isotopomers will be altitude-dependent, and any detailed analysis of the atmospheric data must account for both the kinetic and photolysis components. Further work that compares the model results to observations is in progress.

5. Conclusion

[41] We present a simple and flexible semianalytic model, based on the Born-Oppenheimer approximation and the Reflection Principle, for the photo-induced isotopic fractionation in polyatomic molecules of interest to atmospheric chemistry. Only direct photolysis through a single excited state is treated, other types of photodissociation (predissociation, coupled states photodissociation, and the like) cannot be examined within this formalism. Fortunately, the applicability of the direct photodissociation limit can be tested by comparing the time scales for dissociation and vibration from the experimental data themselves—ideally $\Delta\nu_{h\nu} \gg \nu_{\text{vib}}$, where $\Delta\nu_{h\nu}$ is the full width half maximum of the photodissociation cross section(s) and ν_{vib} is (are) the fundamental vibrational frequency (frequencies).

[42] The small changes of a molecule's ZPE as a function of isotopic substitution have two consequences: displacing the peak of the spectrum by an amount roughly equal to ΔZPE and the modification of the shape of the vibrational wave function. The model quantitatively predicts the dissociation cross section for the isotopologues of the diatomic and triatomic molecules investigated here (HCl, HI, N_2O, O_3), yet is sufficiently simple to be included in detailed chemistry/circulation codes that can be used to examine the sources and sinks of important atmospheric constituents. For example, *Blake et al.* [2003] and *Morgan et al.* [2004] have modeled the stratospheric enrichments of nitrous oxide, and the model values are in good agreement with measurements. This also implies that our understanding of the stratospheric circulation is largely satisfactory. Our model may be generalized to more complex systems by taking the "effective" normal modes of molecules into account. Validity can be checked by comparing the characteristic width to the fundamental vibrational frequency(ies).

[43] **Acknowledgments.** We thank C. D. Camp, M. Gerstell, X. Jiang, V. Natraj, C. D. Parkinson, R. L. Shia, and J. D. Weibel for helpful comments and discussions. We also thank M. S. Johnson for sharing the ab initio calculation of N_2O's cross sections. This work was supported in part by an NSF grant ATM-9903790. The development of the Caltech/JPL 2-D model was supported by NASA grant NAG1-1806.

References

Ascenzi, D., P. M. Regan, and A. J. Orr-Ewing (1999), The ultraviolet photodissociation of DCl: H/D isotope effects on the Cl(^{2}P) atom spin-orbit branching, *Chem. Phys. Lett.*, *310*, 477–484.

Bahou, M., C. Y. Chung, Y. P. Lee, B. M. Cheng, Y. L. Yung, and L. C. Lee (2001), Absorption cross sections of HCl and DCl at 135–232 nanometers, *Astrophys. J. Lett.*, *559*, L179–L182.

Blake, G. A., M. C. Liang, C. G. Morgan, and Y. L. Yung (2003), A Born-Oppenheimer photolysis model of N_2O fractionation, *Geophys. Res. Lett.*, *30*(12), 1656, doi:10.1029/2003GL016932.

Brenninkmeijer, C. A. M., D. C. Lowe, M. R. Manning, R. J. Sparks, and P. F. J. van Velthoven (1995), The ^{13}C, ^{14}C, and ^{18}O isotopic composition of CO, CH_4, and CO_2 in the higher southern latitudes lower stratosphere, *J. Geophys. Res.*, *100*(D12), 26,163–26,172.

Brown, A., and G. G. Balint-Kurti (2000), Spin-orbit branching in the photodissociation of HF and DF. I. A time-dependent wave packet study for excitation from v = 0, *J. Chem. Phys.*, *113*(5), 1870–1878.

Cliff, S. S., and M. H. Thiemens (1997), The $^{18}O/^{16}O$ and $^{17}O/^{16}O$ ratios in atmospheric nitrous oxide: A mass-independent anomaly, *Science*, *278*, 1774–1776.

Cliff, S. S., C. A. M. Brenninkmeijer, and M. H. Thiemens (1999), First measurement of the $^{18}O/^{16}O$ and $^{18}O/^{16}O$ ratios in stratospheric nitrous oxide: A mass-independent anomaly, *J. Geophys. Res.*, *104*(D13), 16,171–16,175.

Connes, P., J. Connes, W. S. Benedict, and L. D. Kaplan (1967), Traces of HCl and HF in the atmosphere of Venus, *Astrophys. J.*, *147*, 1230–1237.

Dahl, J. P. (1983), Dynamical equations for the Wigner functions, in *Energy Storage and Redistributions in Molecules*, edited by J. Hinze, Plenum, New York.

Debergh, C. (1993), The D/H ratio and the evolution of water in the terrestrial planets, *Origins Life Evol. Biosphere*, *23*(1), 11–21.

Donahue, T. M., J. H. Hoffman, R. R. Hodges, and A. J. Watson (1982), Venus was wet—A measurement of the ratio of deuterium to hydrogen, *Science*, *216*, 630–633.

Eiler, J. M., and E. Schauble (2004), $^{18}O^{13}C^{16}O$ in earth's atmosphere, *Geochem. Cosmochim. Acta*, in press.

Frost, R. L., J. E. Beckman, G. D. Watt, G. J. White, and J. P. Phillips (1982), Limits on the D: H mod ratio in the interstellar medium for molecular observations, in *Submillimeter Wave Astronomy*, Cambridge Univ. Press, New York.

Gao, Y. Q., and R. A. Marcus (2001), Strange and unconventional isotope effects in ozone formation, *Science*, *293*, 259–263.

Geiss, J., and H. Reeves (1981), Deuterium in the solar system, *Astron. Astrophys.*, *93*, 1–2.

Huff, A. K., and M. H. Thiemens (1998), $^{17}O/^{16}O$ and $^{18}O/^{16}O$ isotope measurements of atmospheric carbon monoxide and its sources, *Geophys. Res. Lett.*, *25*(18), 3509–3512.

Intergovernmental Panel on Climate Change (IPCC) (2001), *Climate Change: The Scientific Basis*, edited by J. T. Houghton et al., Cambridge Univ. Press, New York.

Irion, F. W., et al. (1996), Stratospheric observations of CH_3D and HDO from ATMOS infrared solar spectra: Enrichments of deuterium in methane and implications for HD, *Geophys. Res. Lett.*, *23*(17), 2381–2384.

Johnson, M. S., G. Billing, A. Gruodis, and M. Janssen (2001), Photolysis of nitrous oxide isotopomers studied by time-dependent hermite propagation, *J. Phys. Chem. A*, *105*, 8672–8680.

Johnston, J. C., and M. H. Thiemens (1997), The isotopic composition of tropospheric ozone in three environments, *J. Geophys. Res.*, *102*(D21), 25,395–25,404.

Kaiser, J., T. Röckmann, C. A. M. Brenninkmeijer, and P. J. Crutzen (2002), Wavelength dependence of isotope fractionation in N_2O photolysis, *Atoms. Chem. Phys. Discuss.*, *2*, 1735–1763.

Kaiser, J., T. Röckmann, and C. A. M. Brenninkmeijer (2003), Assessment of $^{15}N^{15}N^{16}O$ as a tracer of stratospheric processes, *Geophys. Res. Lett.*, *30*(2), 1046, doi:10.1029/2002GL016253.

Kaye, J. A. (1987), Mechanisms and observations for isotope fractionation of molecular species in planetary atmosphere, *Rev. Geophys.*, *25*(8), 1609–1658.

Kim, K. R., and H. Craig (1993), N-15 and O-18 characteristics of nitrous oxide: A global perspective, *Science*, *262*, 1855–1857.

Lämmerzahl, P., T. Röckmann, C. A. M. Brenninkmeijer, D. Krankowsky, and K. Mauersberger (2002), Oxygen isotope composition of stratospheric carbon dioxide, *Geophys. Res. Lett.*, *29*(12), 1582, doi:10.1029/2001GL014343.

Mauersberger, K. (1987), Ozone isotope measurements in the stratosphere, *Geophys. Res. Lett.*, *14*(1), 80–83.

Mauersberger, K., P. Lämmerzahl, and D. Krankowsky (2001), Stratospheric ozone isotope enrichments-revisited, *Geophys. Res. Lett.*, *28*(16), 3155–3158.

McElroy, M. B., N. D. Sze, and Y. L. Yung (1973), Photochemistry of Venus atmosphere, *J. Atmos. Sci.*, *30*(7), 1437–1447.

McElroy, M. B., M. J. Prather, and J. M. Rodriguez (1982), Escape of hydrogen from Venus, *Science*, *215*, 1614–1615.

McLinden, C. A., M. J. Prather, and M. S. Johnson (2003), Global modeling of the isotopic analogues of N_2O: Stratospheric distributions, budgets, and the ^{17}O-^{18}O mass-independent anomaly, *J. Geophys. Res.*, *108*(D8), 4233, doi:10.1029/2002JD002560.

Merienne, M., B. Coguart, and A. Jenouvrier (1990), Temperature effect on the ultraviolet absorption of $CFCl_3$, CF_2Cl_2, and N_2O, *Planet. Space Sci.*, *38*, 617–625.

Miller, C. E., and Y. L. Yung (2000), Photo-induced isotopic fractionation, *J. Geophys. Res.*, *105*(23), 29,039–29,051.

Morgan, C., M. Allen, M. C. Liang, R. L. Shia, G. A. Blake, and Y. L. Yung (2004), Isotopic fractionation of nitrous oxide in the stratosphere: Comparison between model and observations, *J. Geophys. Res.*, *109*, D04305, doi:10.1029/2003JD003402.

Mulliken, R. S. (1971), Role of kinetic energy in the Franck-Condon principle, *J. Chem. Phys.*, *55*, 309–314.

Ogilvie, J. F. (1971), Semi-experimental determination of a repulsive potential curve for hydrogen iodide, *Trans. Faraday Soc.*, *67*, 2205.

Owen, T. (1992), Deuterium in the solar-system, *Symp. Int. Astron. Union*, *150*, 97–101.

Owen, T., B. L. Lutz, and C. Debergh (1986), Deuterium in the outer solar system: Evidence for 2 distinct reservoirs, *Nature*, *320*, 244–246.

Owen, T., J. P. Maillard, C. Debergh, and B. L. Lutz (1988), Deutrium on Mars: The abundance of HDO and the value of D/H, *Science*, *240*, 1767–1770.

Parisse, C., J. Brion, and J. Malicet (1996), UV absorption spectrum of ozone: Study of the isotope effect in the Hartley system, *Chem. Phys. Lett.*, *248*, 31–36.

Prinn, R. G. (1971), Photochemistry of HCl and other minor constituents in atmosphere of Venus, *J. Atmos. Sci.*, *28*(6), 1058.

Rahn, T., and M. Wahlen (1997), Stable isotope enrichment in stratospheric nitrous oxide, *Science*, *278*, 1776–1778.

Rahn, T., H. Zhang, M. Wahlen, and G. A. Blake (1998), Stable isotope fractionation during ultraviolet photolysis of N_2O, *Geophys. Res. Lett.*, *25*, 4489–4492.

Richet, P., Y. Bottinga, and M. Javoy (1977), Review of hydrogen, carbon, nitrogen, oxygen, sulfur, and chlorine stable isotope fractionation among gaseous molecules, *Annu. Rev. Earth Planet. Sci.*, *5*, 65–110.

Röckmann, T., C. A. M. Brenninkmeijer, P. J. Crutzen, and U. Platt (1999), Short-term variations in the $^{13}C/^{13}C$ ratio of CO as a measure of Cl activation during tropospheric ozone depletion events in the Arctic, *J. Geophys. Res.*, *104*(D1), 1691–1697.

Röckmann, T., C. A. M. Brenninkmeijer, M. Wollenhaupt, J. N. Crowley, and P. J. Crutzen (2000), Measurement of the isotopic fractionation of $^{15}N^{14}N^{16}O$, $^{14}N^{15}N^{16}O$, and $^{14}N^{14}N^{18}O$ in the UV photolysis of nitrous oxide, *Geophys. Res. Lett.*, *27*, 1399–1402.

Röckmann, T., J. Kaiser, J. N. Crowley, C. A. M. Brenninkmeijer, and P. J. Crutzen (2001a), The origin of the anomalous or "mass-independent" oxygen isotope fractionation in tropospheric N_2O, *Geophys. Res. Lett.*, *28*, 503–506.

Röckmann, T., J. Kaiser, C. A. M. Brenninkmeijer, J. N. Crowley, R. Borchers, W. A. Brand, and P. J. Crutzen (2001b), Isotopic enrichment of nitrous oxide ($^{15}N^{14}N^{16}O$, $^{14}N^{15}N^{16}O$, $^{14}N^{14}N^{18}O$) in the stratosphere and in the laboratory, *J. Geophys. Res.*, *106*, 10,403–10,410.

Schinke, R. (1993), *Photodissociation Dynamics*, Cambridge Univ. Press, New York.

Selwyn, G., and H. S. Johnston (1981), Ultraviolet absorption spectrum of nitrous oxide as a function of temperature and isotopic substitution, *J. Chem. Phys.*, *74*, 3791–3803.

Stein, L. Y., and Y. L. Yung (2003), Production, isotopic composition, and atmospheric fate of biologically produced nitrous oxide, *Annu. Rev. Earth Planet. Sci.*, *31*, 329–356.

Tonokura, K., Y. Matsumi, M. Kawasaki, S. Tasaki, and R. Bersohn (1992), Photodissociation of hydrogen chloride at 157 and 193 nm: Angular distributions of hydrogen atoms and fine-structure branching ratios of chlorine atoms in the $2P_j$ levels, *J. Chem. Phys.*, *97*(11), 8210–8215.

Turatti, F., D. W. T. Griffith, S. R. Wilson, M. B. Esler, T. Rahn, H. Zhang, and G. A. Blake (2000), Positionally dependent ^{15}N factors in the UV photolysis of N_2O determined by high resolution FTIR spectroscopy, *Geophys. Res. Lett.*, *27*, 2489–2492.

Urey, H. C. (1947), The thermodynamic properties of isotopic substances, *J. Chem. Soc.*, 562–581.

van Harrevelt, R., and M. C. van Hemert (2000), Photodissociation of water. II. Wave packet calculations for the photofragmentation of H_2O and D_2O in the *B* band, *J. Chem. Phys.*, *112*(13), 5787–5808.

Vidal-Madjar, A., R. Ferlet, and M. Lemoine (1998), Deuterium observations in the galaxy, *Space Sci. Rev.*, *84*(1–2), 297–308.

Vogt, R., R. Sander, R. Von Glasow, and P. J. Crutzen (1999), Iodine chemistry and its role in halogen activation and ozone loss in the marine boundary layer: A model study, *J. Atmos. Chem.*, *32*(3), 375–395.

Wigner, E. (1932), On the quantum correction for thermodynamic equilibrium, *Phys. Rev.*, *40*, 749–759.

Yoshida, N., and S. Matsuo (1983), Nitrogen isotope ratio of atmospheric N_2O as a key to the global cycle of N_2O, *Geochem. J.*, *17*(5), 231–239.

Yoshida, N., and S. Toyoda (2000), Constraining the atmospheric N_2O budget from intramolecular site preference in N_2O isotopomers, *Nature*, *405*, 330–334.

Yoshino, K., D. E. Freeman, and W. H. Parkinson (1984), High resolution absorption cross-section measurements of N_2O at 295–299 K, *Planet. Space Sci.*, *32*, 1219–1222.

Yung, Y. L., and W. B. DeMore (1982), Photochemistry of the stratosphere of Venus—Implications for atmospheric evolution, *Icarus*, *51*(2), 199–247.

Yung, Y. L., and R. W. Dissly (1992), Deutrium in the solar-system, *ACS Symp. Ser.*, *502*, 369–389.

Yung, Y. L., and D. M. Kass (1998), Deuteronomy? A puzzle of deuterium and oxygen on Mars, *Science*, *280*, 1545–1546.

Yung, Y. L., and C. E. Miller (1997), Isotopic fractionation of stratospheric nitrous oxide, *Science*, *278*, 1778–1780.

Zhang, H., P. O. Wennberg, V. H. Wu, and G. A. Blake (2000), Fractionation of $^{14}N^{15}N^{16}O$ and $^{15}N^{14}N^{16}O$ during photolysis at 213 nm, *Geophys. Res. Lett.*, *27*(16), 2481–2484.

G. A. Blake, M.-C. Liang, and Y. L. Yung, Division of Geological and Planetary Sciences, California Institute of Technology, MS150-21, 1200 E. California Blvd., Pasadena, CA 91125, USA. (gab@gps.caltech.edu; mcl@gps.caltech.edu; yly@gps.caltech.edu)